J.A. Woodis, EH13
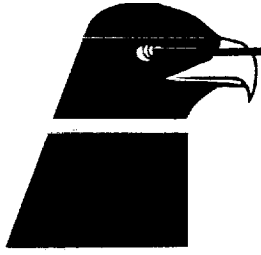
Applied Research, Inc.

Huntsville, Alabama • Arlington, Virginia

"Focused On The Future . . . Committed To Excellence"

Enhanced NDE Systems

Baseline Task Final Report

Juy 28, 1993

Contract NAS8-39394

Enhanced NDE Systems

Baseline Task Final Report

Juy 28, 1993

Contract NAS8-39394

TABLE OF CONTENTS

LIST OF FIGURES

LIST OF TABLES

NDE Final Report

1.0 Contract Goals

The goal of this contractual effort was to evaluate the Langley narrow-band ultrasonic debond detection method for a factory use configuration. Successful accomplishment requires establishing the robustness of the method, and enhancing it if necessary. It is also desirable to strive for simplicity of implementation, such as attachment to in-place scanning devices planned for NDE measurements.

The contract was established with three phases for the ultrasonic work:

Phase 1: Establish the method and robustness of the ultrasonic method.

Phase 2: (Optional) Follow up on any questions which arise with respect to the method or its implementation and produce a Phase A design.

Phase 3: Fabricate and test the Phase A design.

This is a report on Phase 1. In performing this, we have met with Langley personnel at Langley Research Center and in our facilities. We have acquired and utilized their transducer equipment and processing electronics. Also we have received three debond samples from SAIC used in their SPIP program, and utilized at NASA a debond SRM sample manufactured by Morton Thiokol. Our conclusion is that for the first-line debond, the Langley method works well as a robust indicator of bonding anomalies. For the second line debond, it has high potential as a robust indicator. Because of the weakness of the second bond line signal, we recommend that processing techniques be enhanced to increase robustness. This processing for both bond lines can be achieved with the same hardware.

1

2.0   Accomplishments

### 2.1   Acquisition and Conversion of the Langley Hardware

Langley personnel kindly agreed to lend their hardware, to speed up the process. This hardware was brought to our laboratory and set up similarly to their arrangement, except that we established a computer interface. The transducer was a 250 kHz device requiring a several inch water stand-off to separate front surface from deeper returns. This hardware was essentially all analog, producing fast response, but limiting the processing technique and digital enhancement.

A D/A board was added to enable computer control of tone burst length and frequency, which allows frequency scanning. Also a 5 MHz A/D was added to allow signal acquisition of transducer output of higher frequency probes. Such a change was associated with acquisition of a dual ultrasonic transmitter/receiver which allows reception while transmitting, and does not receive the front surface reflection. Such probes are readily available at frequencies around one megahertz, and much more convenient to implement, not requiring the water stand-off.

2.2   Computer Model Development Results

A computer model was written, based on theoretical analysis of a many-layered structure (n + 1 layers, n boundaries) supporting standing plane waves while being ultrasonically driven. The calculations of this model are as presented below in Table 1. It was assumed that the transducer does not receive the front surface reflection and this

2

Table 1. Recursive Algorithm for the Ultrasonic Reflection Coefficient from a Planer Material with n Boundaries
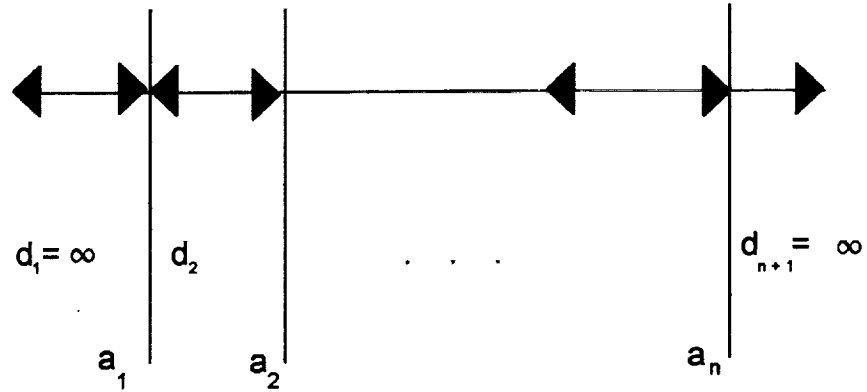
For a planer material with n boundaries at locations $a_1, \ldots a_n$, and n-1 finite layer thickness $d_1 = \infty$, $d_2 = a_2 - a_1, \ldots, d_n = a_n - a_{n-1}$, $d_{n+1} = \infty$

$R_{j\ layers}$ = reflection from boundaries a_j and beyond $(j=1, n-1)$

$$= (R_{j,\,j+1} + R_{j+1}^{\ layers}\ e^{i\,2k_{j+1}d_{j+1}})/(\,1 + (R_{j,\,j+1})\,(R_{j+1}^{\ layers})\,e^{i\,2k_{j+1}d_{j+1}}\,)$$

$$R_n^{\ layers} = R_{n,\,n+1} = (Z_n - Z_{n+1})/(Z_n + Z_{n+1})$$

$$R_{j,\,j+1} = (Z_j - Z_{j+1})/(Z_j + Z_{j+1})$$

$$Z_j = \rho_j c_j$$

To remove first boundary reflection subtract $R_{1,2}$

Steel/Insul/Fuel/Air
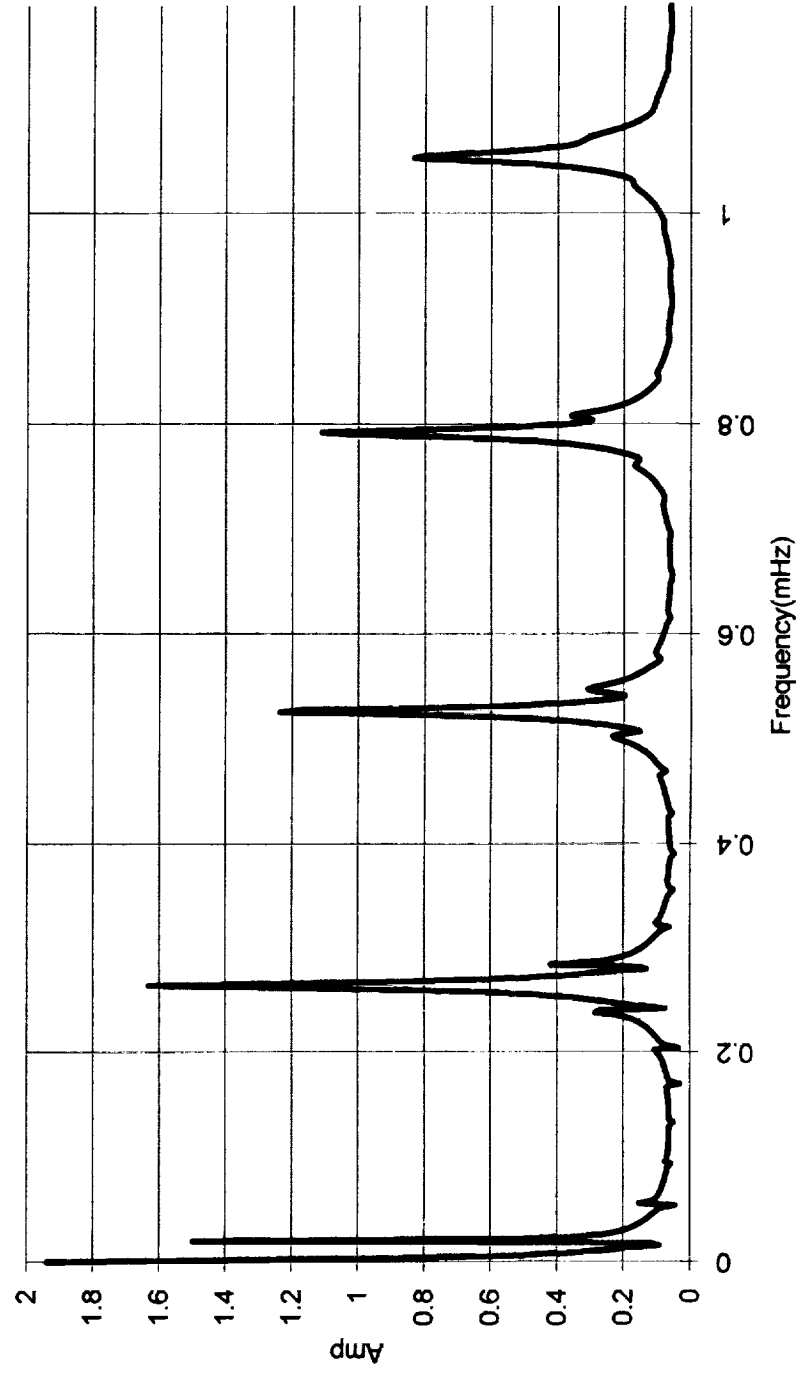
Figure 1 Model Output from Steel with
Front Surface Reflection Subtracted.

4

Steel/Insul/Fuel/Air
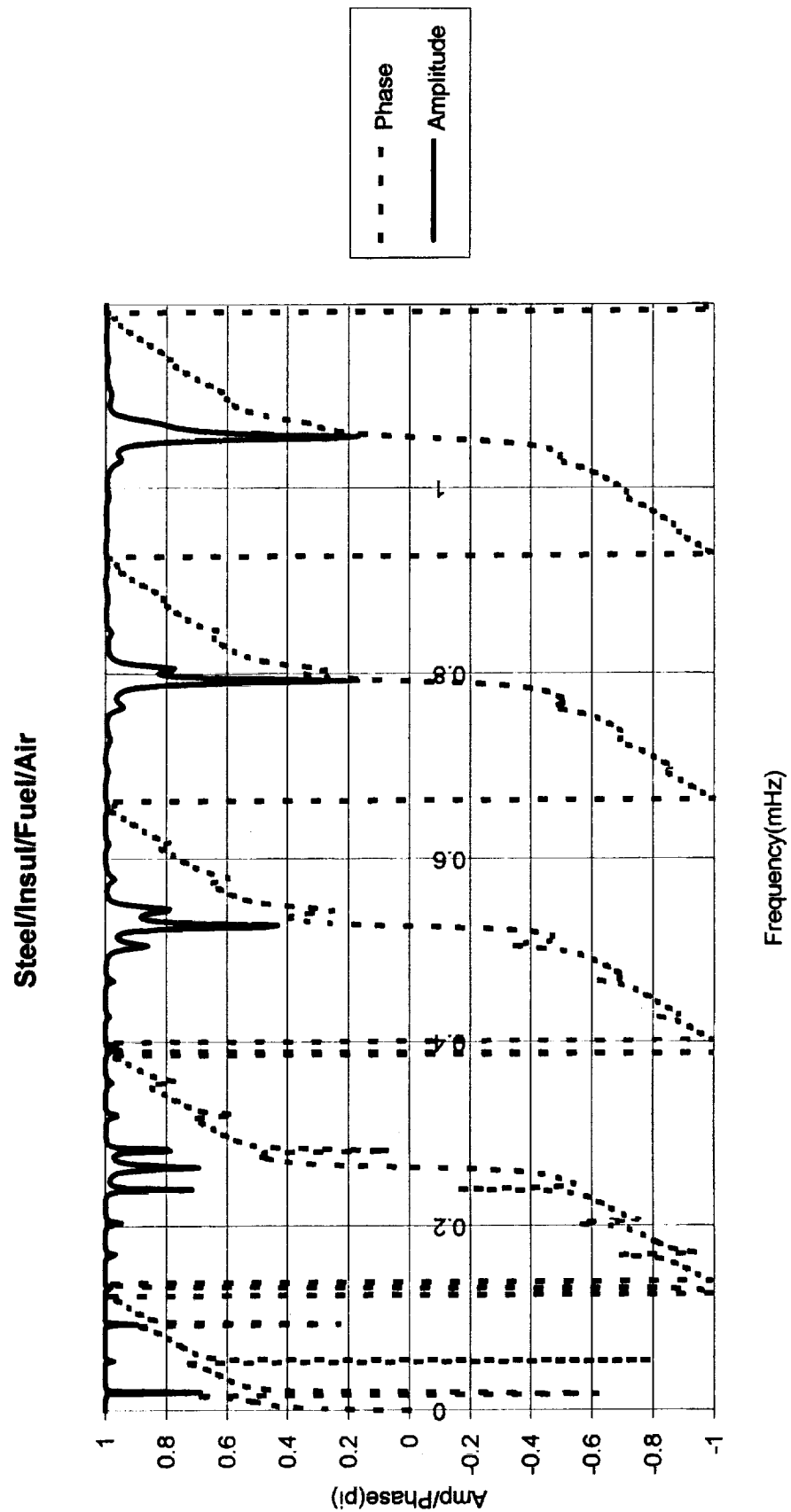
Figure 2 Model Output from Steel with
No Subtraction s

Figure 3 Model Output from Insulation

Langley Figure 1

Figure 4 Model Output to Compare with Langley Model

7

Figure 5 Bond-Debond Signal Variation with Insulation Thickness at First Steel Harmonic .240 MHz

8

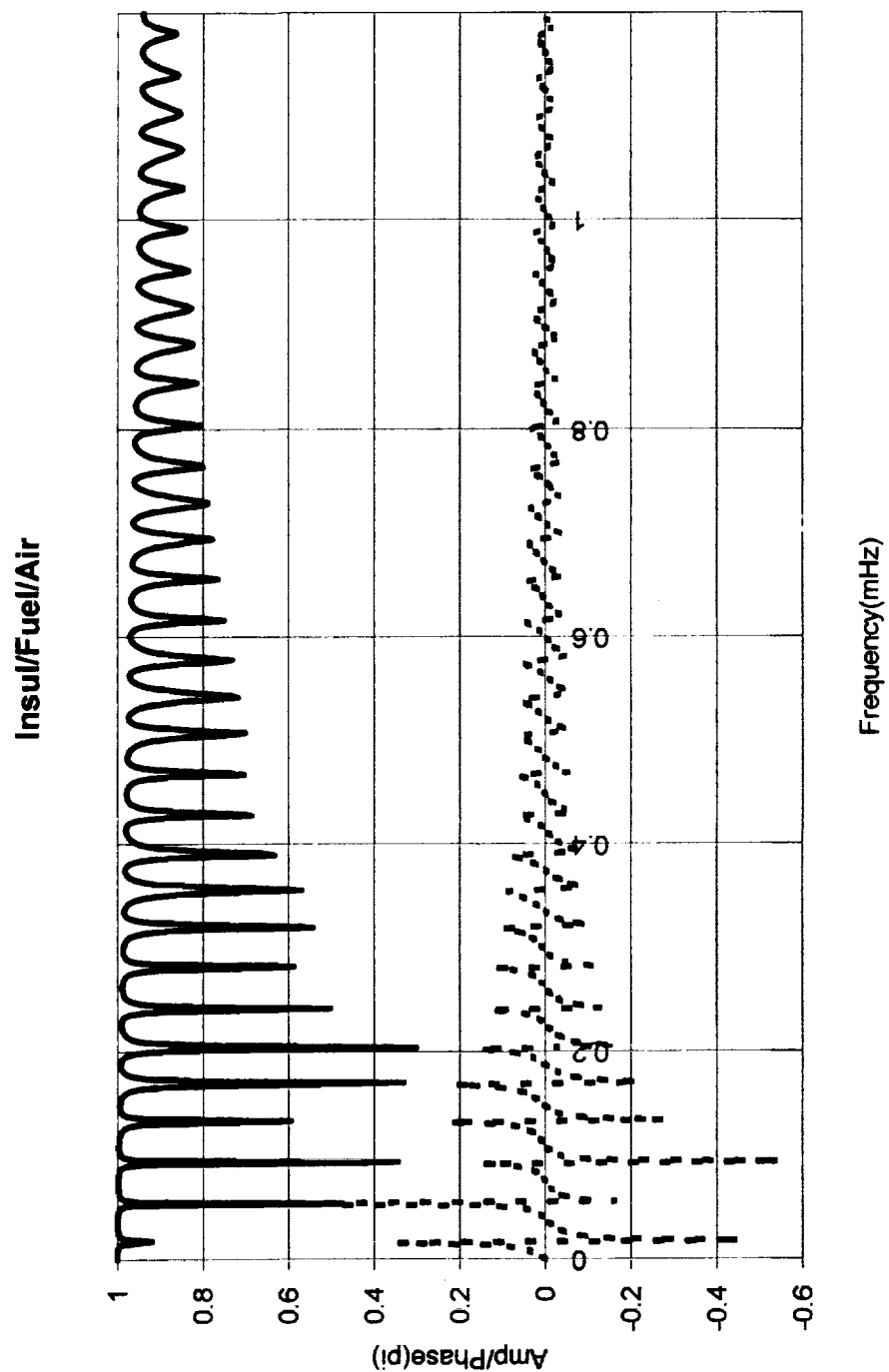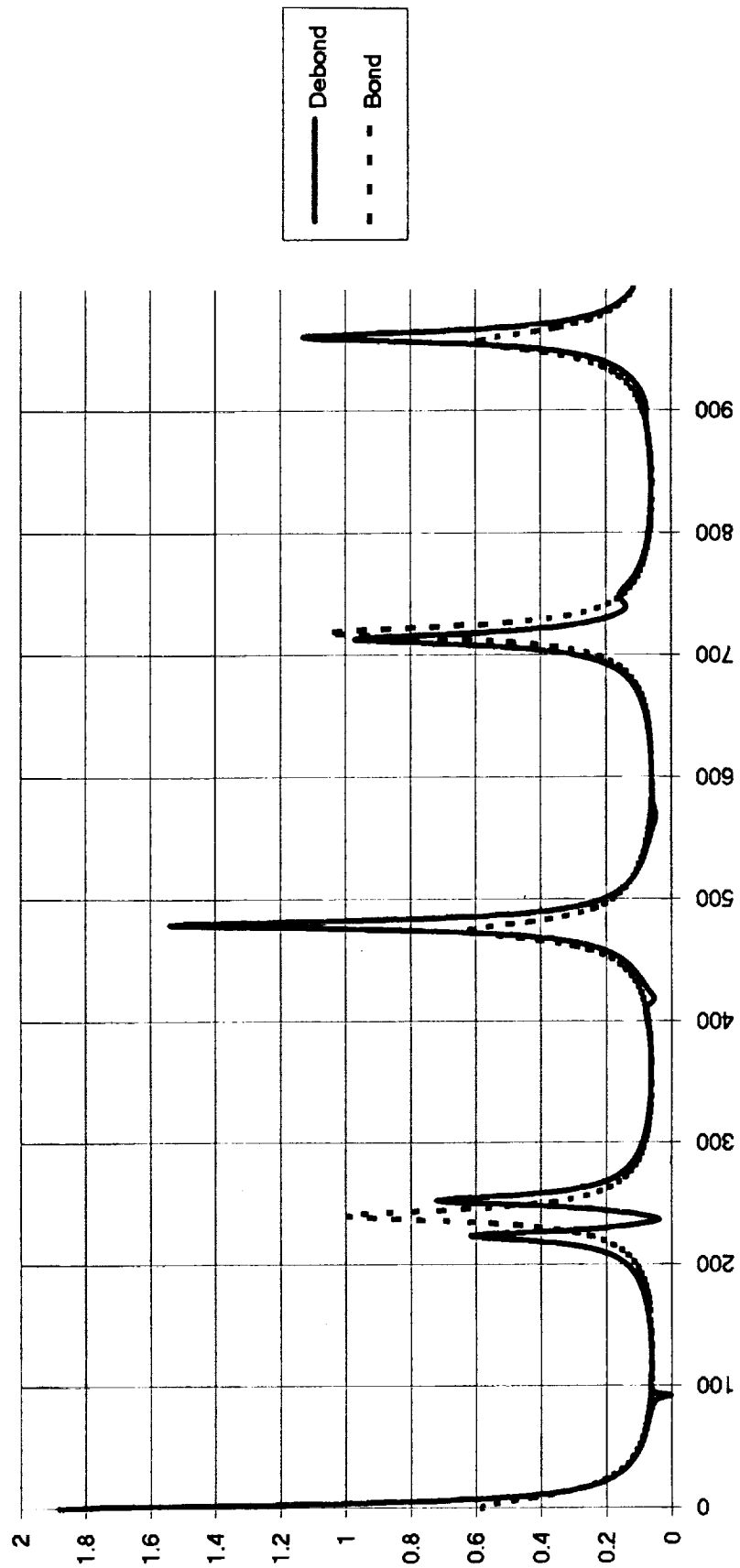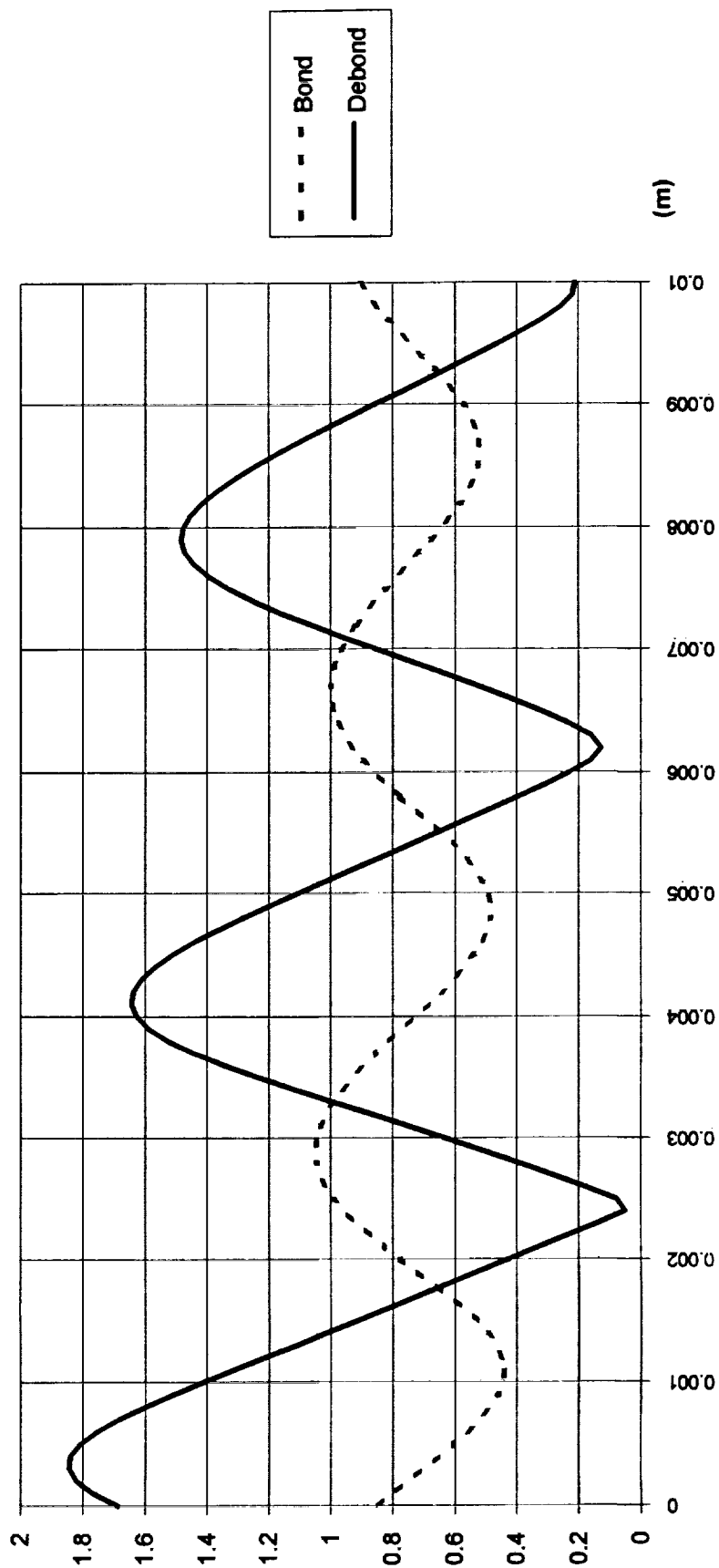was subtracted from the signal received in layer 1. Figures 1 through 3 show typical model output from the layered structure: steel .015m, insulation .005m, fuel .023m, and air. Figure 1 shows the amplitude (reflection coefficient $R_{12}{}^{layers}$) from the total structure, with the front surface reflection, R_{12} subtracted. Figure 2 shows the amplitude (without any subtraction) and phase which reflects from the structure at the steel front surface. The amplitude is positive and the phase covers the range (-1, +1) in Π units. Figure 3 shows the same parameters for the second layer as would be measured interior to the steel. Such parameters can be produced for any layer. Their value is that features in the output can be related to sub-layer features, such as the splitting features around the first steel harmonic in Figure 1 which are related to, and a measure of, the insulation thickness as seen from Figures 2 and 3.

This model describes the system while it is being driven, and the initial state of the system during ring-down (after driving ceases). In applying this model to ring-down, it was assumed that initial tendencies persist. This model was compared with the Langley paper[1] which implemented a different calculation approach, to check for errors. Figures 4 and 5 of this paper are model outputs based on the same parameters as Figures 1 and 2 of the Langley paper, and they agree.

Figure 4 shows that some harmonic amplitudes depend upon whether there is a second-line debond, and is a basis for its detection. Figure 5 shows that the relative sizes of these amplitudes depend sensitively on the insulation thickness and which harmonic is observed. Thus it is possible, for certain insulation thicknesses, to discern the presence of second-line debonds with these amplitudes. However, with a second-line debond, this shows that the signal may be lower or higher than the good bond

---

[1] Madaras, Eric I, et. al., "Detection of Bond line Delaminations in Multilayer Structures with Lossy Components", 1987 Ultrasonics Symposium, p. 1047.

signal. With manufacturing variation, it may be difficult to know the various widths precisely enough in practice, based on specification; hence a point width measurement is desired. For the first layer, the width is trivial to determine by conventional pulsed methods. For the second layer this information sometimes shows up in the scanned spectrum as narrow lines or line splitting, as in Figure 1. Such information must be sought and utilized to predict the significance of the signal. On the other hand, instead of prediction one can search for a difference in signal from surroundings, but the magnitude of this difference is not assured. In any case, it is clear that the second line debond signal is small and must be sought with care.

2.3   Data Acquisition

Besides various samples of steel and aluminum which were available, specific samples related to rocket motor structures were used. A "stepped sample" with regions which successively add layers of insulation, liner, and simulated fuel to the steel layer was used. Samples from the SPIP program with first and second-line debonds were measured. Finally, a large SRM sample with first and second-line debonds, manufactured by Morton-Thiokol was measured.

The stepped sample was measured at the three harmonics at .57, .79, and 1.05 MHz. Both the ring-down area and the driven amplitude were measured at the resonances. Results given in Table 2 are the average of ten measurements, each in a region whose center varies by less than .5 inch. Thus, the variations presented do not represent mainly material variations, but signal generation, acquisition, and processing variations. The numbers relative to the first layer signal are shown for comparison. These figures show little difference between ring-down area and driven resonance amplitude. There is seen the expected variation with harmonic observed, discussed

Table 2. Stepped Sample Results
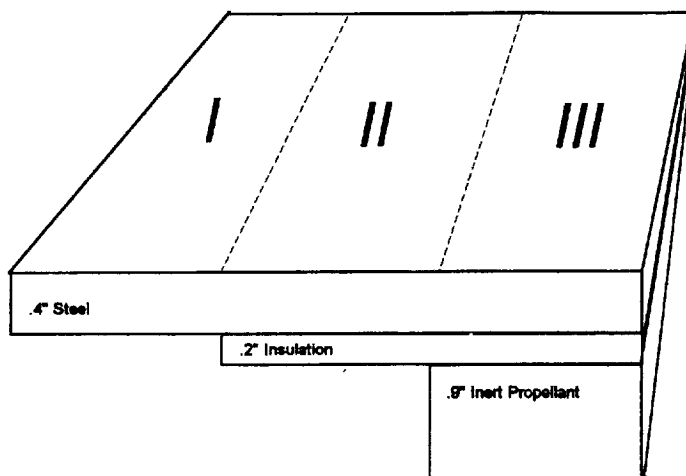
Signals (in equal arbitrary units)

	I		II		III	
	Mean	Std Dev	Mean	Std Dev	Mean	Std Dev
Harmonic 2, .57 MHz						
Toneburst Ringdown	40.19164	1.83898	25.1067	0.84449	22.2293	0.68975
Driven Resonance Amplitude	274.73	13.8093	182.939	4.34257	173.948	5.76716
Harmonic 3, .79 MHz						
Toneburst Ringdown	185.867	4.56318	103.296	0	86.7581	2.635775
Driven Resonance Amplitude	1172.4	25.328	708.736	44.1668	612.531	15.8573
Harmonic 4, 1.05 MHz						
Toneburst Ringdown	82.3511	3.01692	67.0215	2.09788	65.1716	1.86974
Driven Resonance Amplitude	709.768	27.3444	565.336	21.5485	555.84	16.7593

Signal (Relative to Layer 1 Signal)

	I		II		III	
	Mean	Std Dev	Mean	Std Dev	Mean	Std Dev
Harmonic 2, .57 MHz						
Toneburst Ringdown	100.0	4.5	62.4	2.1	55.2	1.7
Driven Resonance Amplitude	100.0	5.0	66.6	1.6	63.3	2.1
Harmonic 3, .79 MHz						
Toneburst Ringdown	100.00	2.5	55.3	3.9	46.6	1.4
Driven Resonance Amplitude	100.0	2.2	60.5	3.8	52.2	1.4
Harmonic 4, 1.05 MHz						
Toneburst Ringdown	100.0	3.6	81.3	2.5	79.1	2.3
Driven Resonance Amplitude	100.0	3.8	79.6	3.0	78.0	2.4

11

with Figure 5. In this case, the third harmonic is slightly more sensitive to bond line character.

The SPIP program samples have debond geometries as described in Figure 6. Display of measurements is done with Figures 7-9. Figure 7 shows ringdown area readings at the second steel harmonic as the height of columns relative to background columns with no height. This sample is made with a first-line debond. There is no significance to the gray level. Figure 8 shows driven resonance amplitude measurements on the same sample at the second harmonic. Figure 9 shows the ringdown area following a single one megahertz pulse on the same sample. All these measurements show the debond displaced slightly from the sample center.
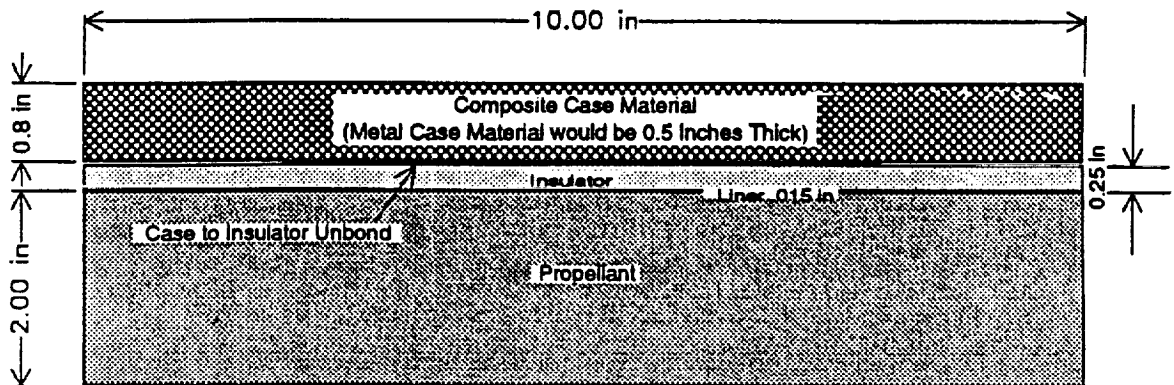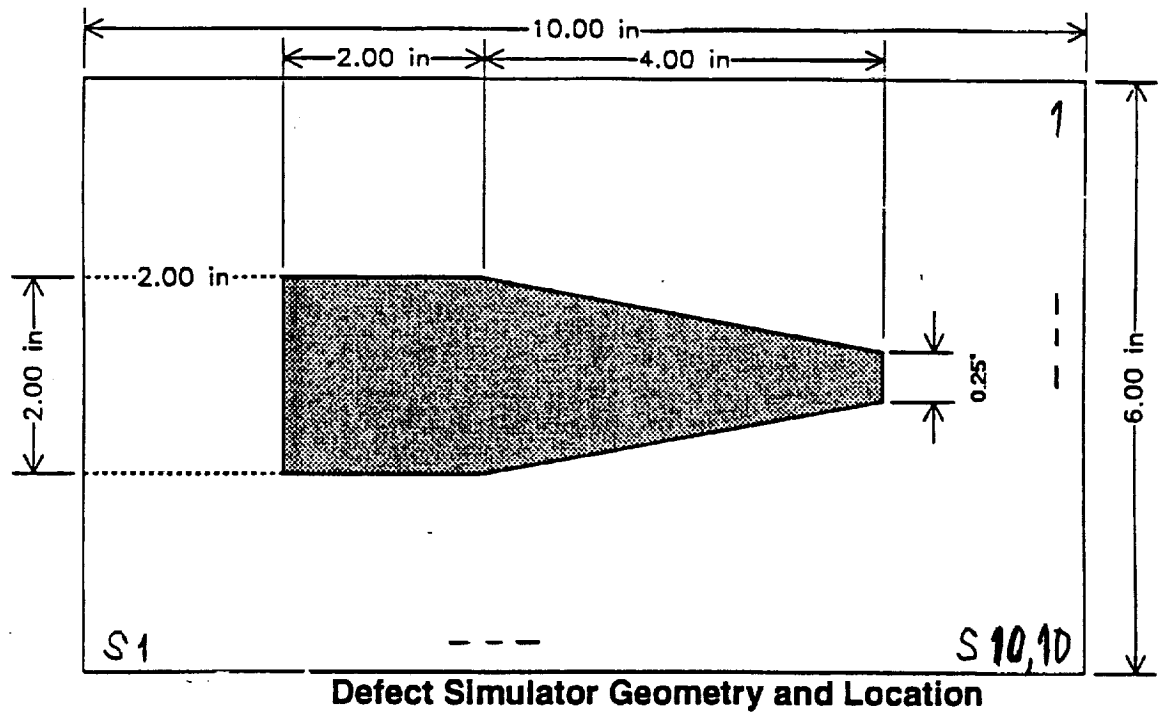
Figure 10 shows measurements made on a first-line debond manufactured in a sample by Morton Thiokol using pull tabs. Again, columns show results relative to background. The technique used here and for Figure 11 is ring-down area following a single pulse.

Figure 11 shows results made on a second-line debond area within the Morton-Thiokol sample. Notice these data are smaller than good bond readings.

2.4   Alternative Processing Methods

Three methods indicative of the bond integrity have been demonstrated: the ring-down area following tone burst, the ring-down area following a single pulse, and the amplitude at resonance during excitation. Other methods include harmonic analysis following a single pulse, use of a narrow single pulse which bounces off the second bond line, generation of a resonance in the insulation, and phase and spectral

Defect Simulator Geometry and Location

**Defect Simulator Geometry and Location
(Case to Insulator Unbond)**

Figure 6. SPIP Sample Geometry
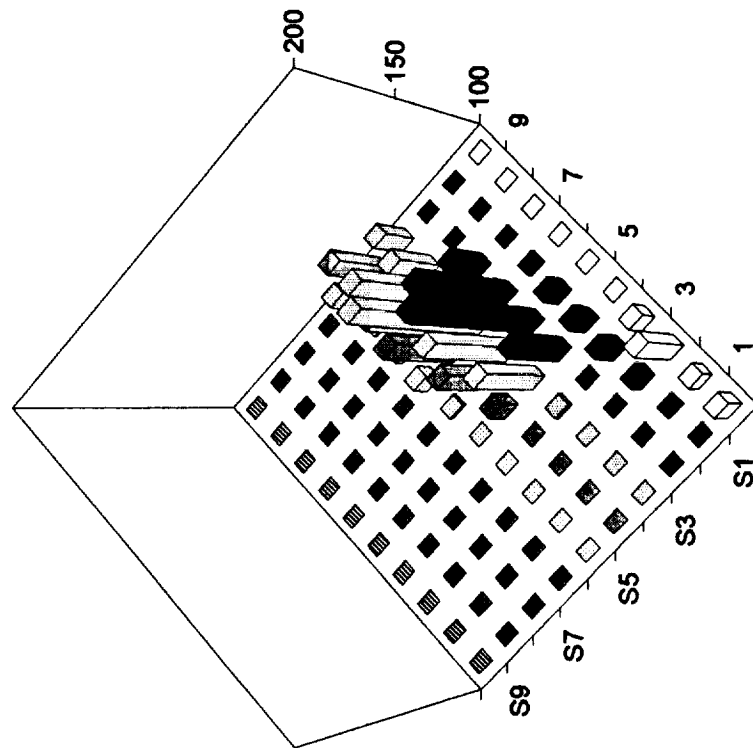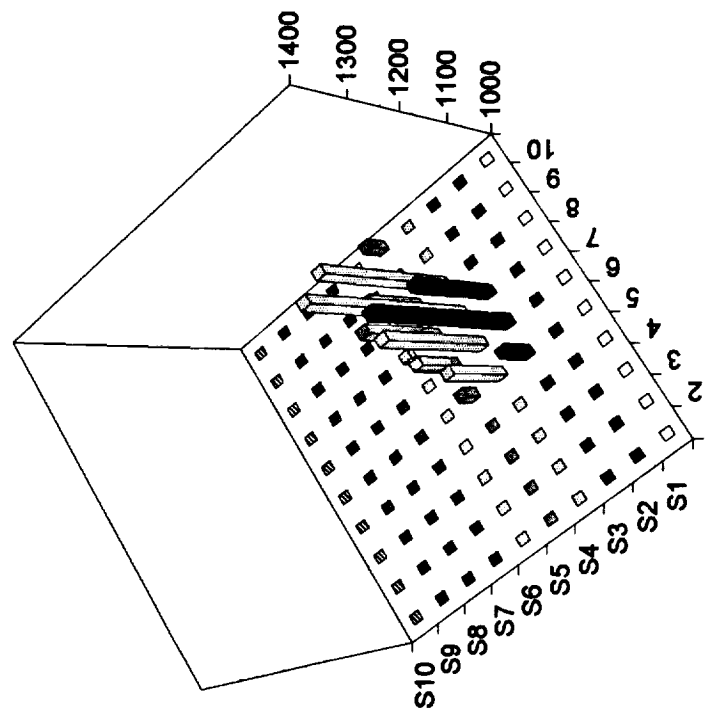
1/4" FLAT RINGDOWN RESONANCE AREA.
SECOND HARMONIC (.92 Mhz)

Figure 7 SPIP Sample
First-line Debond - Toneburst Ringdown

1/4" FLAT DRIVEN RESONANCE AMP.
SECOND HARMONIC (.94Mhz)

Figure 8 SPIP Sample
First-Line Debond - Driven Resonance Amplitude

1/4 Inch Case SPIP First-Line Debond

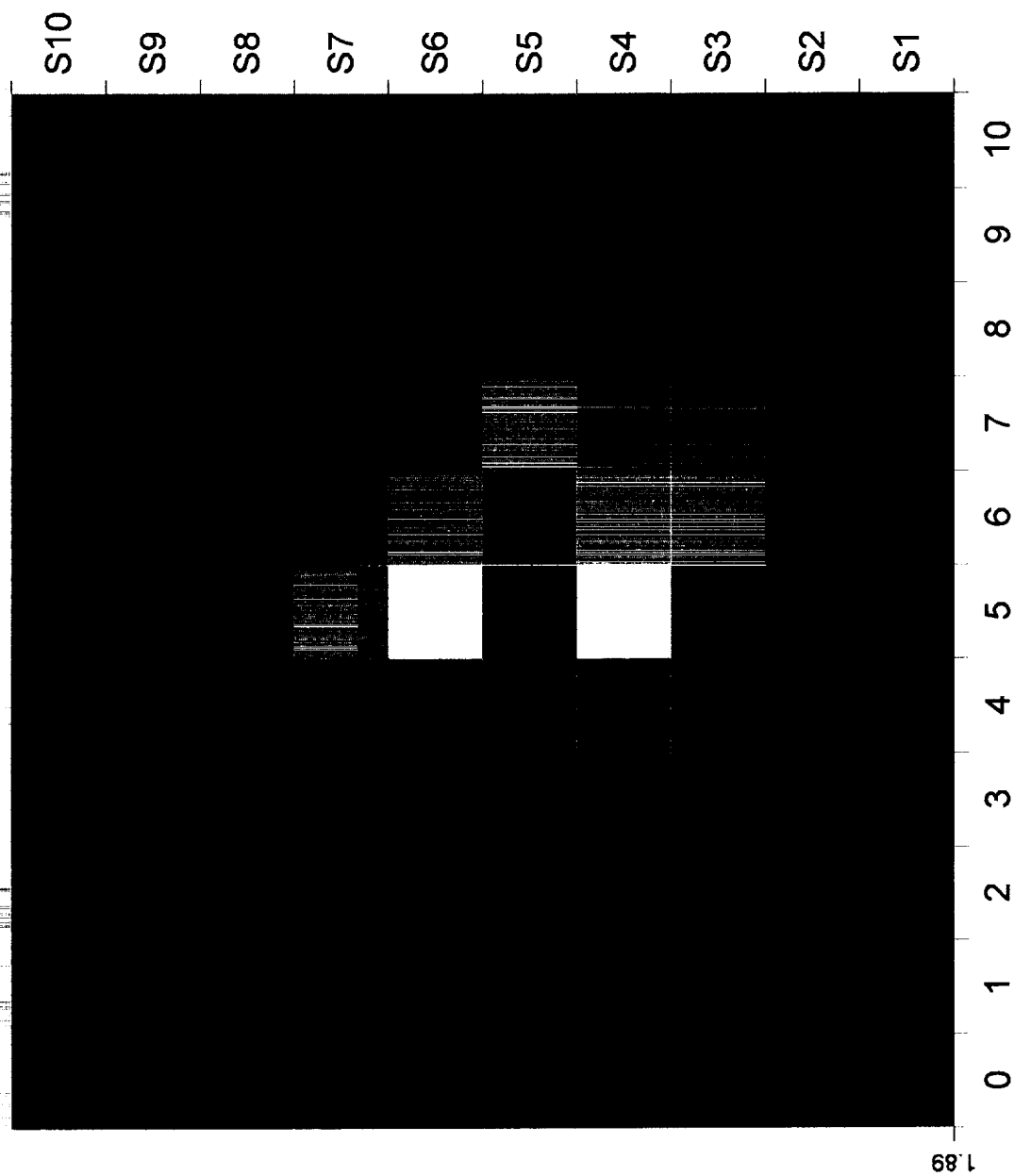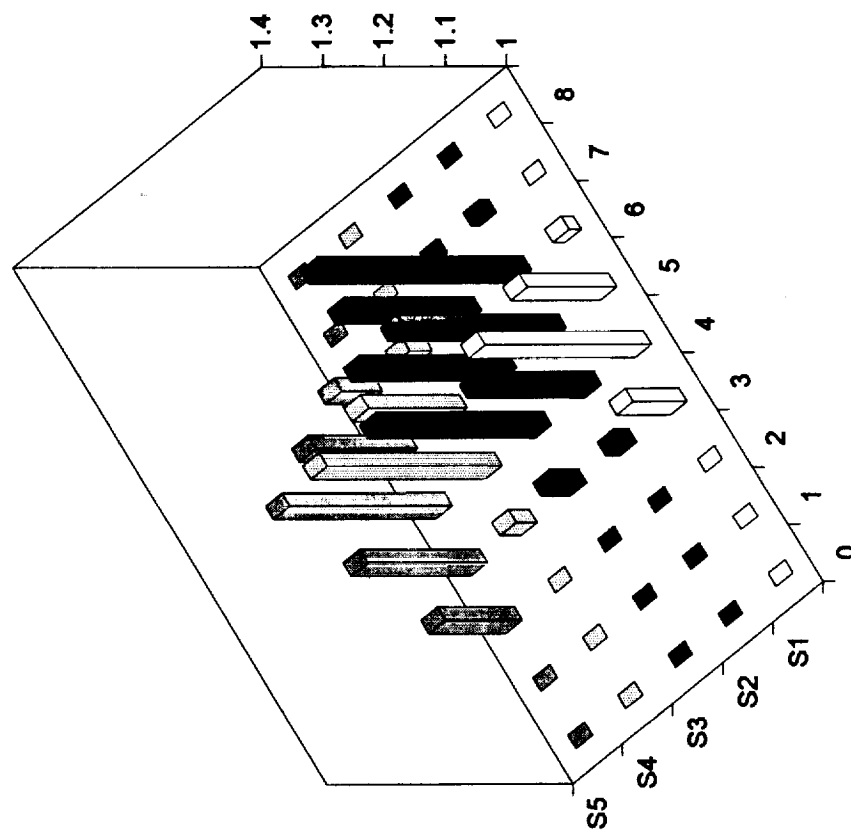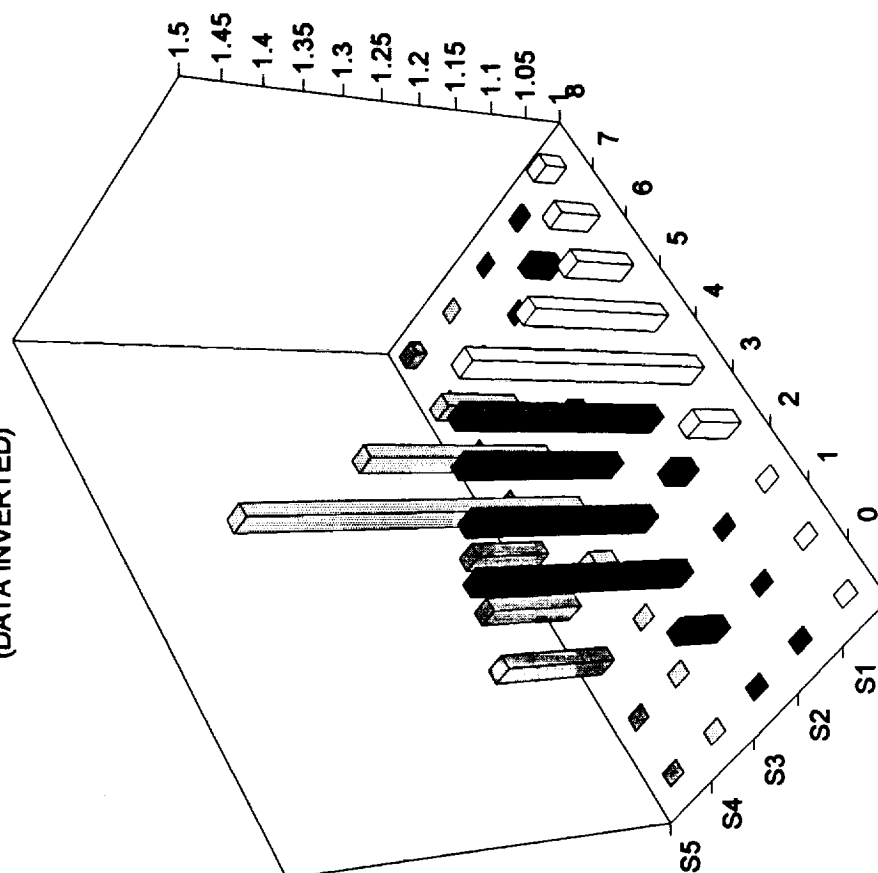**Figure 9. SPIP Sample First-Line Debond - One Cycle Ringdown**

BIG SAMPLE 1st LINE DEBOND (1CYCLE AREA)

Figure 10 Morton Thiokol Sample
First Line Debond

17

BIG SAMPLE 2nd LINE DEBOND (1CYCLE AREA)

(DATA INVERTED)

Figure 11 Morton Thiokol Sample
Second Line Debond

measurement of the totally reflected signal. These methods, including ways of normalizing the signal, provide a dozen methods of processing the signal. Various of the methods have also been analyzed, each having some degree of bond information and some degree of independence. Given the low level of the second-line debond signal, the use of several of these methods concurrently can provide a robust bond line analysis. Signal generation and processing hardware for accomplishing this is not difficult to achieve.

3.0   Implementation

Configuration of this ultrasonic hardware is conceived to be as shown in Figure 12. The sensor could be attached to other scanning apparatus, while the transducer is carried on a skate support which is capable of adjusting the contact pressure, as shown in the inset.

4.0   Conclusions

The tone burst ring-down method and its relative methods contain significant information about the character of the first and second bondlines. Since the second bondline signal is small, several relatively independent techniques (spin-offs of the main technique) could provide enhanced robustness, when processed with neural or fuzzy logic.

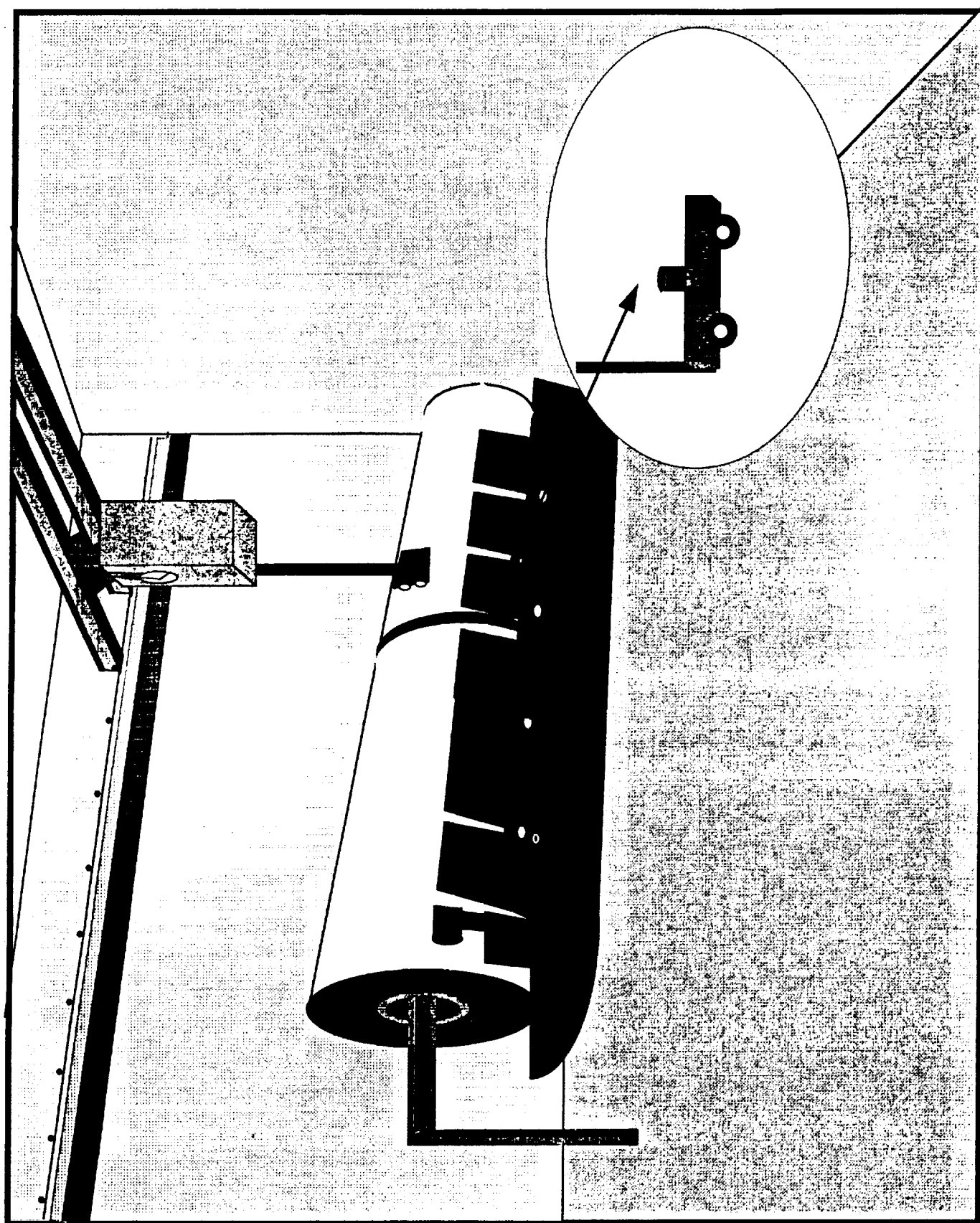A manufacturing floor design involving analog and digital processing is required. Implementation involving attachment to in-place scanning devices is envisioned.

Figure 12 Implementation Concept